Open wind tunnel experiments of the DarkO tail-sitter longitudinal stabilization with constant wind

Florian Sansou, Fabrice Demourant, Gautier Hattenberger, Thomas Loquen, Luca Zaccarian

Open wind tunnel experiments of the DarkO tail-sitter longitudinal stabilization with constant wind ⋆

Florian Sansou * **Fabrice Demourant** **
Gautier Hattenberger * **Thomas Loquen** ** **Luca Zaccarian** ***

* *Ecole Nationale de L'Aviation Civile (ENAC), Toulouse, France, (e-mail: firstname.lastname@recherche.enac.fr).*
** *ONERA DTIS, 2 avenue Edouard Belin, Toulouse, France (e-mail: firstname.lastname@onera.fr)*
*** *Department of Industrial Engineering, University of Trento, Italy, and LAAS-CNRS, Université de Toulouse, CNRS, Toulouse, France, (e-mail: zaccarian@laas.fr)*

Abstract: We describe an experimental platform for testing the DarkO tail-sitter drone in an open wind tunnel experiment. The DarkO convertible UAV is developed and 3D printed at the Ecole Nationale de l'Aviation Civile (ENAC), in Toulouse (France). The objective of the experimental platform is to allow testing control laws in a realistic and secure context. We propose a test bench with a single degree of freedom corresponding to the drone pitch axis. We design a linear proportional/integral feedback hovering stabilizer in the presence of constant wind, and we illustrate its effectiveness in stabilizing a hovering position through experimental results.

Keywords: UAVs, Tail-sitter, Hovering, Linear robust control.

1. INTRODUCTION

Convertible drones have the ability to take off or land vertically and fly like an airplane. They are promising architectures providing energy efficient flight capabilities for strong endurance, as compared with classical coplanar UAVs, like quadcopters. Nevertheless, their electromechanical design and the ensuing control system is still an active research area. A model-free control technique has been used in Olszanecki Barth et al. (2020), which allows avoiding the cumbersome modeling effort, but is clearly prone to the well-known improvements stemming from a careful model-aware solution. When the model is taken into account, one may rely on nonlinear dynamic inversion and incremental nonlinear dynamic inversion techniques (see, e.g., Smeur et al. (2019); Silva et al. (2018); Tal and Karaman (2022)). However, wind is rarely addressed directly by these controllers. The main problem lies in the complexity of estimating the wind relative to the sensor, which cannot be kept in the wind stream.

Virtual flight tests (VFT) allow reliably studying UAV behaviour, due to the realistic experimental conditions, but also protect the model from disastrous accidents. VFT are controlled wind tunnel tests with models fixed to a support for preventing accidental falls, while leaving one or more degrees of freedom free to evolve according to the actual dynamics of the device. Many works have been carried out on this subject, and many of them are cited in the review (Huang and Wang, 2015), which discusses the advantages of VFT over other test methods, such as numerical simulation, software-in-the-loop and hardware-in-the-loop. The forces and moments generated by the aerodynamic effects are real, and consequently their actions on the control surfaces are measurable. Several objectives are identified when using VFT such as aerodynamic model identification, stability limits estimation, etc. At the moment, only a few drones have been tested in virtual flight testing conditions, but the tool is interesting for convertible drones such as tail-sitters. As the studies show (Saeed et al., 2018), (Ducard and Allenspach, 2021), architecture is complex to model because of the many nonlinearities, but it is of great energetic interest. Thus, we propose here to use virtual test flights as a follow-up work to the preliminary results reported in (Sansou and Zaccarian, 2022), regarding a tail-sitter convertible UAV, called DarkO, designed and developed at the Ecole Nationale de l'Aviation Civile (ENAC) in Toulouse (France) (Barth et al., 2020), (Bronz et al., 2020). A sketch of the DarkO UAV is shown on Fig. 1.

This paper reports on the prototype set up to carry out virtual flight tests for the DarkO drone, as illustrated in Section 3. In particular, we discuss how the longitudinal motion of the DarkO can be effectively experimented, while the translational motion is simulated using a software-in-the-loop extension, which is necessary because of the fixed mount only enabling one rotational motion of the UAV. A second contribution reported in Section 4 is to extend the linear control scheme proposed in (Sansou and Zaccarian, 2022) to a PI-like structured output feedback capable of coping with non-zero wind facing the DarkO. Indeed, we

⋆ Research supported in part by ONERA-ISAE-ENAC Research Federation (FONISEN - PCGN) and by Occitanie region.

report on the controller architecture and two gain-tuning techniques, ensuing different level of wind disturbance rejection. Simulation results in Section 4 present a H_∞-based tuning method. Experiments are reported in Section 5.

2. MODEL OF THE DARKO UAV

DarkO is assembled from multiple 3D printed Onyx parts (a robust material comprising omnidirectional carbon fibres). Its actuators consist in two propellers symmetrically placed at the front of the wing and two elevons, placed at the back of the wing, acting as redundant control surfaces.

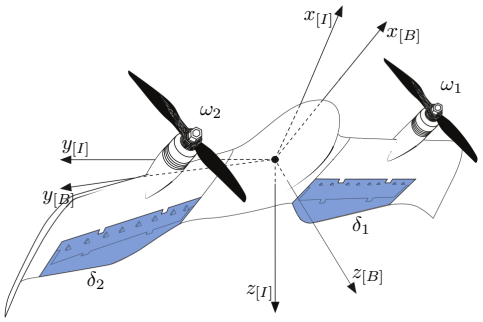

Fig. 1. The DarkO convertible UAV with its inertial and body frames, and a schematic representation of the actuators.

As shown on Fig. 1, we may model the position and attitude of the DarkO by using an inertial reference frame "$[I]$" linked to the earth's surface, and a body reference frame "$[B]$" attached to the drone, with $x_{[B]}$ corresponding to the roll axis (the propellers axes), $y_{[B]}$ being the pitch axis (the direction of the wings) and $z_{[B]}$ being the yaw axis. According to the notation in Lustosa et al. (2019) the left and right propeller/elevon are denoted by subscripts $i = 1$ (left) and $i = 2$ (right), respectively.

In this paper, we extend the linear controller proposed in (Sansou and Zaccarian, 2022) to take into account constant wind when the UAV is hovering. We may simplify the full nonlinear model (described in (Sansou, 2022, eqn (2.10), p. 25)) by neglecting some aerodynamic effects, namely all the terms that are quadratic in the speed $\boldsymbol{v_b}$ and $\boldsymbol{\omega_b}$. We perform this simplification in order to obtain a model representing the hovering stabilization, which implies a zero linear and angular velocity for the UAV. We keep the aerodynamic effects induced by the air flow generated by the propellers.

$$\dot{\boldsymbol{p}} = \boldsymbol{v}, \qquad \dot{\boldsymbol{q}} = \frac{1}{2}\boldsymbol{q} \otimes \boldsymbol{\omega_b} \tag{1a}$$

$$m\dot{\boldsymbol{v}} = m\boldsymbol{g} + R(\boldsymbol{q})Fu + R(\boldsymbol{q})D_{\mathrm{f}}(\delta)R^\top(\boldsymbol{q})\|\boldsymbol{w}\|\boldsymbol{w}, \tag{1b}$$

$$J\dot{\boldsymbol{\omega}}_{\mathrm{b}} = -\left[\boldsymbol{\omega}_{\mathrm{b}}\right]_\times J\boldsymbol{\omega}_{\mathrm{b}} + Mu + D_{\mathrm{m}}(\delta)R^\top(\boldsymbol{q})\|\boldsymbol{w}\|\boldsymbol{w}. \tag{1c}$$

In (1), $\boldsymbol{p} \in \mathbb{R}^3$ is the position of the centre of mass (CoM) expressed in the inertial frame and $\boldsymbol{v} \in \mathbb{R}^3$ denotes its velocity. $\boldsymbol{g} = [0\ 0\ g]^\top$ is the (constant) gravity vector, $\boldsymbol{q} = \left[\eta\ \boldsymbol{\epsilon}^\top\right]^\top$ is a unit quaternion charactering the attitude, in order to avoid the gimbal lock problem and $\boldsymbol{\omega}_{\mathrm{b}}$ is the rotational speed expressed in the body frame. Finally, $m \in \mathbb{R}$ is the mass and $J \in \mathbb{R}^{3\times3}$ is the inertia. The transformation from $[B]$ to $[I]$ is realized by a rotation matrix constructed from the quaternion with the well know formula: $R(\boldsymbol{q}) = I + 2\eta\left[\boldsymbol{\epsilon}\right]_\times + 2\left[\boldsymbol{\epsilon}\right]_\times^2$, where the "skew" operator is define as $[u]_\times v = u \times v$ for any $u, v \in \mathbb{R}^3$. The constant matrices F and M and the control vector u appearing in (1) are defined in (Sansou and Zaccarian, 2022) and are recalled below

$$u := [\tau_1\ \tau_2\ \delta_1\tau_1\ \delta_2\tau_2]^\top = k_{\mathrm{f}}\left[\omega_1^2\ \omega_2^2\ \delta_1\omega_1^2\ \delta_2\omega_2^2\right]^\top \tag{2}$$

$$F := \begin{bmatrix} a_{\mathrm{f}} & a_{\mathrm{f}} & 0 & 0 \\ 0 & 0 & 0 & 0 \\ 0 & 0 & b_{\mathrm{f}} & b_{\mathrm{f}} \end{bmatrix} \quad M := \begin{bmatrix} a_{\mathrm{m}} & -a_{\mathrm{m}} & b_{\mathrm{m}} & -b_{\mathrm{m}} \\ 0 & 0 & c_{\mathrm{m}} & c_{\mathrm{m}} \\ d_{\mathrm{m}} & -d_{\mathrm{m}} & 0 & 0 \end{bmatrix} \tag{3}$$

with the following coefficients

$$\left[\begin{array}{c|c} a_{\mathrm{f}} & b_{\mathrm{f}} \\ \hline a_{\mathrm{m}} & b_{\mathrm{m}} \\ \hline c_{\mathrm{m}} & d_{\mathrm{m}} \end{array}\right] = \left[\begin{array}{c|c} 1 - \frac{S}{4S_{\mathrm{p}}}C_{\mathrm{d}_0} & -\frac{S}{4S_{\mathrm{p}}}C_{\mathrm{l}0}\xi_{\mathrm{f}} \\ \hline \frac{k_{\mathrm{m}}}{k_{\mathrm{f}}} & \frac{S}{4S_{\mathrm{p}}}a_y C_{\mathrm{l}_0}\xi_{\mathrm{f}} \\ \hline \frac{S}{4S_{\mathrm{p}}}\Delta_{\mathrm{r}}C_{\mathrm{l}_0}\xi_{\mathrm{m}} & p_y + \frac{S}{4S_{\mathrm{p}}}a_y C_{\mathrm{d}_0} \end{array}\right]$$

with the numerical values of the scalar quantities reported in (Sansou, 2022, Table 1, p. 61).

We can define the wind vector expressed in the inertial reference frame $[I]$: $\boldsymbol{w} = [w_x\ w_y\ w_z]^\top$ which is reduced, for our longitudinal motion experiments to $\boldsymbol{w} = [w_x\ 0\ 0]^\top$. Following the derivations in (Sansou, 2022, eqn (2.24) and (2.25)), the expressions of the input-dependent matrices D_{f} and D_{m} associated with the wind effects is computed as:

$$D_{\mathrm{f}}(\delta_i) := -\frac{1}{4}\rho S\Phi^{(\mathrm{fv})}\left(\begin{bmatrix}0\\ \xi_f\\ 0\end{bmatrix}_\times \delta_1 + \begin{bmatrix}0\\ \xi_f\\ 0\end{bmatrix}_\times \delta_2 - 2I\right)$$

$$D_{\mathrm{m}}(\delta_i) := -\frac{1}{4}\rho S\left(\left(\begin{bmatrix}0\\ a_y\\ 0\end{bmatrix}_\times \Phi^{(\mathrm{fv})} + B\Phi^{(\mathrm{mv})}\right)\begin{bmatrix}0\\ \xi_m\\ 0\end{bmatrix}_\times \delta_1 + \left(\begin{bmatrix}0\\ -a_y\\ 0\end{bmatrix}_\times \Phi^{(\mathrm{fv})} + B\Phi^{(\mathrm{mv})}\right)\begin{bmatrix}0\\ \xi_m\\ 0\end{bmatrix}_\times \delta_2 - 2B\Phi^{(\mathrm{mv})}\right)$$

where

$$\left[\ \Phi^{(\mathrm{fv})}\ \middle|\ \Phi^{(\mathrm{mv})}\ \right] := \left[\begin{array}{ccc|ccc} C_{\mathrm{d}_0} & 0 & 0 & 0 & 0 & 0 \\ 0 & 0 & 0 & 0 & 0 & -\frac{\Delta_{\mathrm{r}}}{c}C_{\mathrm{l}_0} \\ 0 & 0 & C_{\mathrm{l}_0} & 0 & 0 & 0 \end{array}\right],$$

with the numerical values of the scalar quantities reported in (Sansou, 2022, Table 1, p.61).

The linearized dynamics about an equilibrium $(\boldsymbol{p_{eq}}, \boldsymbol{v_{eq}}, \boldsymbol{\epsilon_{eq}}, \boldsymbol{\omega_{eq}})$ correspond to

$$\dot{\tilde{\boldsymbol{x}}} = A\tilde{\boldsymbol{x}} + G\tilde{\boldsymbol{u}} \tag{4}$$

with the incremental state $\tilde{\boldsymbol{x}}$ and input $\tilde{\boldsymbol{u}}$ defined as

$$\tilde{\boldsymbol{x}} := [\boldsymbol{p} - \boldsymbol{p_{eq}}\ \boldsymbol{v}\ \boldsymbol{\epsilon} - \boldsymbol{\epsilon_{eq}}\ \boldsymbol{\omega_b}]^\top \qquad \tilde{\boldsymbol{u}} := \boldsymbol{u} - \boldsymbol{u_{eq}},$$

and the expressions for A and G defined in (Sansou and Zaccarian, 2022, Proposition 1 and (7)).

3. TEST BENCH PRESENTATION

3.1 Motivation for the design

Closed-loop simulations with the controller developed in (Sansou and Zaccarian, 2022), show that in the presence of constant horizontal wind in the $(x_{[B]}, z_{[B]})$ plane, the UAV changes its pitch angle. This behaviour has also been observed in wind tunnel tests with the experimental device. Intuitively speaking, a reduced angle of attack leads to a smaller surface area facing the wind, so as to reduce the drag force, which strongly impacts the position. At the same time, the air flow due to the constant wind

generates lift, compensated by a reduced propeller thrust and a consequent reduction of the UAV consumption. The goal of the prototype described here is to evaluate experimentally the effect of the wind on the DarkO device.

3.2 Physical description, sensing, and actuation

The developed prototype comprises 3D printed parts in Onyx and PLA (polylactic acid, a thermoplastic polyester). It is especially designed for running experiments in front of a wind tunnel with responses that resemble those of the DarkO due to the similar shape (see Fig. 3). The central part, which contains the onboard avionics (autopilot, GPS, etc.) in the DarkO, has been here replaced by a one-degree of freedom revolute joint (see Fig. 2). The wings are the same as those of the DarkO, with the electronic speed controllers (ESC), governing the brushless motor speed, placed in the wings. As described in Section 3.1, we wish to represent and study the y-axis degree of freedom of the DarkO UAV. The main carbon tube linking the two wings is used as the rotation axis. This tube is fixed to two bearings placed 28.5 mm apart in order to obtain a solid fixation of the rig. This rotation axis is equipped with an optical quadrature rotary encoder to accurately measure the orientation of the device. The advantage of this sensor is that it does not produce torque on the rotation axis. This encoder offers 4000 edges per revolution, which results in a resolution of $0.09°/pulse$.

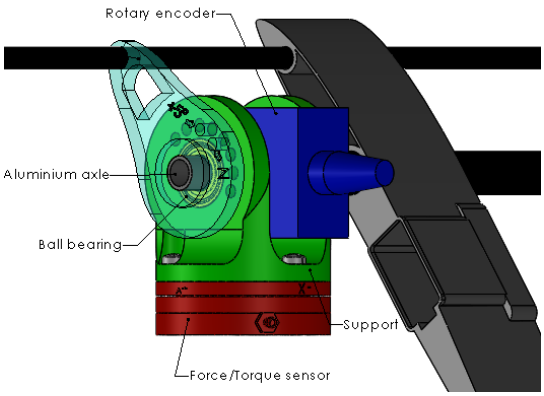

Fig. 2. The one degree-of-freedom joint.

As shown in Fig. 2, the indexer and the holder are drilled so that the rotation can be locked at known positions (0°, 90°, etc.) by a screw on the indexer that fits into the holes of the holder. Locking the device allows for a correct initialization of the incremental encoder. Locking also allows placing the device in specific exact positions in order to identify the aerodynamic coefficients.

The pivoting joint is also equipped with a 6 degrees of freedom (DOF) force-torque sensor, providing a measurement of the internal wrench exerted on the experimental device by the support. The experimental test bench is also equipped with a hot wire to measure the airspeed seen by the drone.

The photo reported in Fig. 3 shows the experimental device in its test environment. The drone is placed in front of an open wind tunnel, called WindShape, generating a horizontal wind between 2 and 16 $\mathrm{m\,s^{-1}}$. Thus, during our

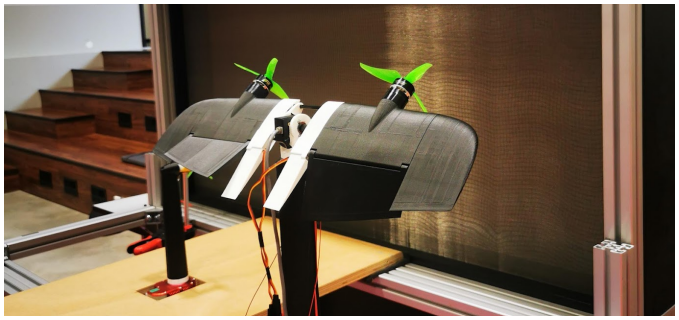

Fig. 3. Single degree-of-freedom DarkO model in front of the WindShape.

tests, we consider the vertical wind component to be zero. The drone is placed at the centre of the WindShape, in the most laminar flow area, while the hot wire sensor is placed as close as possible to the drone.

The geometry of the experimental setup allows placing the power and signal cables close to the centre of rotation so as to minimize their frictional effects on the structure. Despite this fact, the rotation system inevitably interferes with the drone, by creating parasitic forces, notably drag. The projected surface of the joint is small compared to the wing surface, so that the drag generated by this support is low compared to the drag of the wing and the propellers, thus it can be neglected.

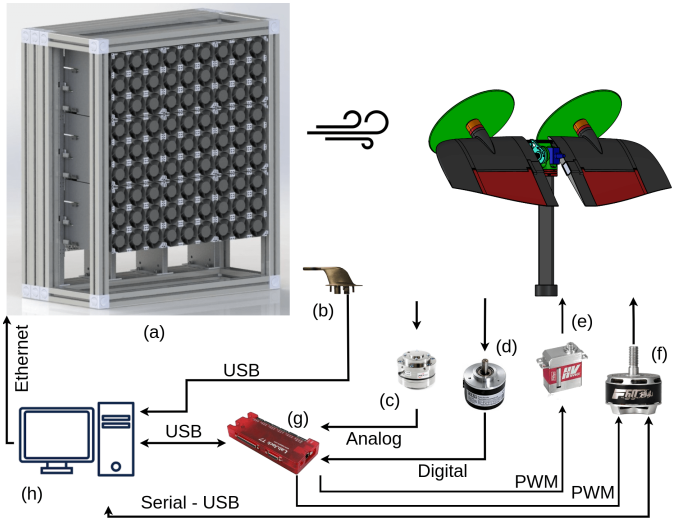

Fig. 4. Virtual flight testing architecture: WindShape (a); Airspeed sensor (b); Force/Torque sensor (c); Rotary encoder (d); Servomotor (e); Brussless motor + ESC (f); LabJack (g); Control computer (h)

A schematic diagram of the functional subcomponents of the experimental device and their interconnection is shown in Fig. 4, which is explained below by referring to the various subsystems with their corresponding letter (a)-(i).

The motors (f) are powered by an external 12v 20Ah battery and the servo motors (e) are powered by 5v via a LabJack T7 (LabJack, 2001) acquisition module (g). The LabJack module (g) concentrates most of the sensing/actuating signals: six analog inputs for the force/torque sensor (c), two digital quadrature inputs for

the rotary encoder (d), one analog input (or serial link depending on the sensor) for the airspeed sensor (b), two digital PWM (Pulse Width Modulation) outputs for the motors (f) and two digital PWM outputs for the servomotors (e). The elevons are driven by servomotors that do not provide a position measurement signal, therefore we use the setpoint, assuming a perfect actuator, which is reasonable, due to the software saturation imposed on the elevons commanded input and the correct sizing of the servomotors with respect to the involved forces.
The LabJack (g) has an application programming interface (API), allowing for a remote connection with a computer. We have developed a Python code that communicates with the LabJack in order to retrieve the sensor values, compute the command to be applied to the actuators according to the control scheme presented below, and generate the output signals for the actuators. The data collected from the LabJack is recorded to be used for post-processing and generate the plot reported in Section 5.
To generate the wind, we use a WindShape device, which also has an API, allowing it to be controlled through an Ethernet network. The developed Python code can assign the WindShape wind speed and therefore act on the model. It is thus possible to test a set of hovering configurations and their associated transients in the same test campaign, without any action on the model.

3.3 Software-in-the-loop translational motion

Since the prototype is connected to the fixed support, it is not possible to experimentally reproduce the translational motion. We have instead included a software-in-the-loop routine that simulates the translational motion by integrating the force measurements available at the joint. In particular, the translational velocity (resp. position) of the UAV is obtained by single (resp. double) integration of the data measured by the force sensor. We neglect the aerodynamic influence of the (simulated) speed on the wing for the sake of simplicity. In particular, from equations (1a) and (1b), we obtain the simplified model

$$\dot{\boldsymbol{v}} = \boldsymbol{g} + \frac{1}{m}\left(R(\boldsymbol{q})(F\boldsymbol{u} + D_{\mathrm{f}}(\delta)R^{\top}(\boldsymbol{q})\|\boldsymbol{w}\|\boldsymbol{w})\right) \tag{5a}$$

$$= \boldsymbol{g} + \frac{1}{m}\boldsymbol{F}_{meas}, \tag{5b}$$

where $\boldsymbol{F}_{meas}$ represents the forces measured by the sensor in the bias-corrected inertial reference frame. To calibrate the bias correction, at the initialization, the measured forces are averaged over 6000 samples, the model being blocked at a steady position (pitch angle at 0°, namely vertical orientation). Removing the bias from the measured force at each measurement, we subtract the gravity effect on the model from the measurement. An artificial mass m is instead assigned to the software-in-the-loop dynamics according to (5b), which allows testing several configurations to better appreciate the influence of the drone's mass on possible transient saturation events. This allows investigating scenarios involving the nontrivial mass of the battery, which is not present in our model. Although this manipulation is easy, it does not represent perfectly the reality because we do not take into account the distribution of the masses in the drone and thus the inertia modifications. The transitional velocity and position of the UAV are then obtained by single and double numerical integration of the acceleration as in (5), using a trapezoidal numerical integration.

4. INTEGRAL-BASED LINEAR CONTROL

In our previous work (Sansou and Zaccarian, 2022, III.B) we proposed a proportional feedback stabilizing a hovering position in the absence of wind (perturbation). We propose here an extension including integral action, suitable for operating with a non-measured perturbation represented by a constant wind. The objective is to stabilize the drone at the reference position, rejecting the unknown constant wind disturbance.

4.1 Description of the control scheme

We experiment the situation with the wind only acting along the $x_{[I]}$ axis, with the drone oriented towards the wind, i.e. with zero roll and yaw angles. In this configuration, the wind only acts on the linear velocity along the $x_{[B]}$ and $z_{[B]}$ axes, and it only generates a moment about the $y_{[B]}$ axis. A careful inspection of the control and the disturbance input matrices F, M in (3) suggests an effective control architecture to reject a constant disturbance. Indeed, the ailerons and the propellers can be used symmetrically to generate respectively a moment about the $y_{[B]}$ axis and a force along the $x_{[B]}$ axis, thus compensating the disturbance effect. Nevertheless, there is still a force along the $z_{[B]}$ axis to be compensated, and an integral action can asymptotically converge to the desired force, even with a non-measured wind disturbance w. We may thus stabilize the UAV at a hovering position, different from the zero-wind equilibrium. The control solution exploits the pitch angle degree of freedom, for compensating the wind effect.

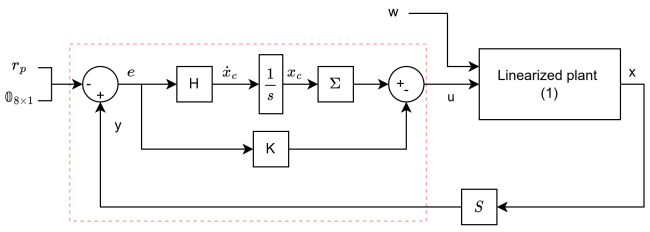

Fig. 5. Proposed integral-based controller.

The proposed controller, shown in Fig. 5, corresponds to

$$\dot{x_c} = H(y - \begin{bmatrix} r_p \\ \mathbb{0}_{8\times1} \end{bmatrix}), \tag{6}$$

$$y = Sx, \tag{7}$$

$$u = \Sigma x_c + K(y - \begin{bmatrix} r_p \\ \mathbb{0}_{8\times1} \end{bmatrix}), \tag{8}$$

$$S = \begin{bmatrix} \mathbb{I}_7 & \mathbb{0}_{7\times5} \\ \mathbb{0}_{4\times8} & \mathbb{I}_4 \end{bmatrix}, \tag{9}$$

$$\Sigma = \begin{bmatrix} 1 & 1 & 0 & 0 \\ 0 & 0 & 1 & 1 \end{bmatrix}^{\top}, \tag{10}$$

where $x_c \in \mathbb{R}^2$ is the integrator state; $r_p \in \mathbb{R}^3$ is the constant reference comprising a target position for the translational motion; S is an output selection matrix, which removes the pitch angle component from the measured output (impacting only the quaternion linearization) to form y; Σ is an input allocation matrix that allows assigning the first component of the integrator state to

the motor control and the second component to the elevon control. K, H are constant stabilizing gains to be selected in such a way that the linear closed loop matrix

$$A_{cl} = \begin{bmatrix} A & \mathbb{0}_{12\times 2} \\ HS & \mathbb{0}_{2\times 2} \end{bmatrix} - \begin{bmatrix} G \\ \mathbb{0}_{2\times 4} \end{bmatrix} \left(K \left[S \ \mathbb{0}_{11\times 2} \right] - \left[\mathbb{0}_{4\times 12} \ \Sigma \right] \right), \tag{11}$$

characterizing the linearized closed loop be Hurwitz, to ensure stabilization with the linearized dynamics related to the zero-wind scenario (4).

In a nutshell, matrix (11), describes the closed loop shown in Fig. 5: an output feedback with 11 outputs, consisting of the three positions, the three linear velocities, two out of three angles (ϕ and ψ) and the three angular velocities. This structure can be seen as a MIMO proportional-integral solution resulting from a careful observation of the UAV linearized dynamics, which allows a minimal number of integrators embedded in the controller. This control should allow constant disturbances rejection while having a satisfactory robustness. The gain K corresponds to the proportional term and the gain H weights the integral term, inducing convergence to the target. The allocation matrix Σ leads to a symmetrical use of the propellers and ailerons. We must then tune K and H to obtain a satisfactory trade-off between robustness and disturbance rejection. We implement a multi-objective synthesis based on an H_∞ optimization method, described next.

4.2 H_∞-based optimization

To perform a robust selection of K and H, we first characterize several transfers functions in Fig. 5. The measurement output y is used for feedback, the input u is the sum of the integral input Σx_c and the proportional action Ke. The output z corresponds to the output performance signals to control (e, w, u, y, r_p). Thanks to weighting functions $W = \text{diag}(W_1, ..., W_4)$, the design of H and K aims to reject a low frequency perturbation or step w acting on y. In short, the design goal is to bring y to zero despite the low frequency disturbance on w.

From the Nyquist criterion, we know that the margin corresponds to the minimal distance between the singularity (real point -1) and the product between the controller (C) and the plant (P). Consequently, we define the input modulus margin as $MM_u = \min_{\omega\in R} |1 - CP|$ and the output modulus margin as $MM_y = \min_{\omega\in R} |1 - PC|$ for a positive feedback. We first introduce the output sensitivity function $T_{r\to\epsilon} = S_y = (1 - PC)^{-1}$, so that $\|S_y\|_\infty = MM_y^{-1}$ and the input sensitivity function $T_{d\to u} = S_u = (1 - CP)^{-1}$, so that $\|S_u\|_\infty = MM_u^{-1}$. Consequently, the minimization of the H_∞-norm of S_u or S_y, leads to improving the input and output modulus margins. As our system is MIMO, we give importance to both the input and output sensitivity functions, because they do not commute. We also define the transfer functions $T_{r\to u} = CS_y = S_u C$ and $T_{w\to y}$. In order to guarantee a satisfactory trade-off between robustness and performance, we select the weighting functions W_1, W_2, W_3 and W_4 linked to $\|W_1 T_{r\to\epsilon}(s)\|_\infty \leq 1$ and $\|W_2 T_{d\to u}(s)\|_\infty \leq 1$, corresponding to robustness margins at the inputs and outputs, $\|W_3 T_{r\to u}(s)\|_\infty \leq 1$ limiting the control effort, $\|W_4 T_{w\to y}(s)\|_\infty \leq 1$ ensuring suitable wind disturbance rejection. Specifically, the weighting functions are tuned as

$$W_1 = 0.5, \quad W_2 = 0.5, \quad W_3 = 0.8, \quad W_4 = 0.5. \tag{12}$$

The values of W_1 and W_2 ensure $MM_u > 6\ dB$ and $MM_y > 6\ dB$, W_3 and W_4 are tuned to obtain a satisfactory trade-off between the different specifications. The weight W_4 allows managing, among other things, the speed of the rejection.

With selections (12), we cast the design problem for K and H as an H_∞ synthesis under order constraint, providing good input and output specifications for the closed loop:

$$\min_C \left\| \begin{matrix} W_1 T_{r\to\epsilon}(P,C) \\ W_2 T_{d\to u}(P,C) \\ W_3 T_{r\to u}(P,C) \\ W_4 T_{w\to y}(P,C) \end{matrix} \right\|_\infty, \text{ subject to}$$
$$C \in \mathbb{R}^{11\times 4} \text{ stabilizes } P \text{ internally}, \tag{13}$$

where P is the augmented plant containing the integral action and the linearized UAV dynamics. In addition, we impose constraints on the gains K and H ensuring that the closed loop with experimental device only evolves in the (x,z) plane, compatibly.

We solved (13) using Systune (Apkarian and Noll, 2006). Based on non-smooth optimization, Systune dealing with several non-convex scenarios, such as the structured control architecture where we optimize the gain matrices K, H. The optimization algorithm returns optimized selections of

$$\begin{bmatrix} H \\ \hline K \end{bmatrix} = \left[\begin{array}{cccccccccc} -1.902 & 0 & 7.201 & -9.043 & 0 & 33.244 & 0 & 0 & 0 & 4.696 & 0 \\ 0.425 & 0 & -1.620 & 2.024 & 0 & -7.480 & 0 & 0 & 0 & -1.045 & 0 \\ \hline 0.035 & 0 & -0.728 & -1.853 & 0 & -4.445 & 0 & 0 & 0 & -0.323 & 0 \\ 0.035 & 0 & -0.728 & -1.853 & 0 & -4.445 & 0 & 0 & 0 & -0.323 & 0 \\ 0.217 & 0 & -0.164 & 1.074 & 0 & -0.527 & 0 & 0 & 0 & -0.773 & 0 \\ 0.217 & 0 & -0.164 & 1.074 & 0 & -0.527 & 0 & 0 & 0 & -0.773 & 0 \end{array}\right] \tag{14}$$

Introducing a closed-loop spectral abscissa $\alpha = -0.2381$ for A_{cl} in (11).

5. EXPERIMENTAL RESULTS

Fig. 6 shows an experiment of the closed loop in Fig. 5 with the gain selection (14) and a piecewise constant and increasing selection of the horizontal wind w (lower trace). Despite some oscillation, the drone maintains its position in spite of the wind, by suitably tilting the pitch angle. The experimental oscillations are absent in our simulations, suggesting the presence of unmodeled phenomena.
We also observe a behaviour that may be important for future investigations: the drone seems to stabilize more easily along the vertical axis than along the horizontal axis. As expected, as the wind increases, the tilt angle decreases, thus changing the required thrust and elevons deflection. Indeed, the wind generates lift on the wings, which compensates for the gravity effect, and thus the required thrust becomes lower. For each value of w, the model converges to an equilibrium, whose precise mathematical characterization is subject of future work. It is therefore necessary to extend the robustness of the controller by performing a multimodel optimization of the controller. It is also possible to remove the constraints on the controller structure in order to give it more degrees of freedom in the optimization.
The link `https://youtu.be/ce4_FUzeVzI` shows a video of the system of the experimental results.

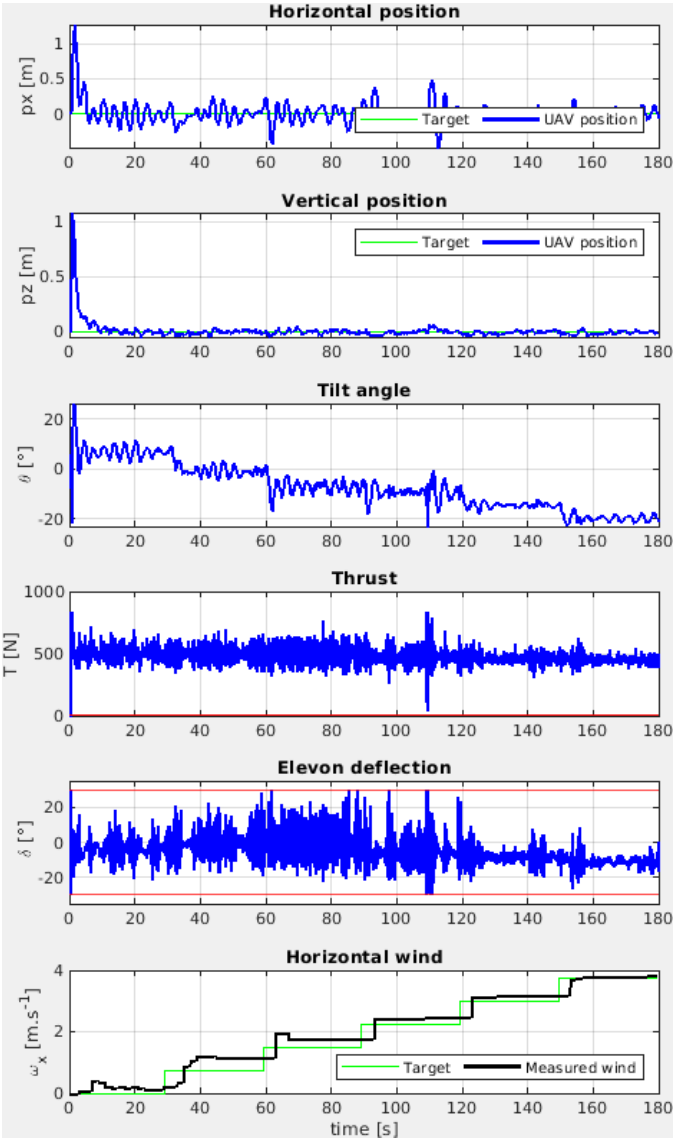

Fig. 6. Experimental results.

6. CONCLUSION

We have described a VFT system for the DarkO convertible drone in a wind tunnel. The goal of this method is to test the control system on a faithful representation of the longitudinal dynamics, while simulating the translational dynamics. We have also presented a PI-based output feedback linear controller for hovering stabilization in a constant wind regime. The controller gains have been optimized using non-convex optimization. The results of the experimental tests show potential for stabilizing the hovering equilibrium in the tested wind speed range, however alternative control architectures should be investigated in the future to address undesired oscillations. Future work also involves performing free flights to validate the reliability of the VFT results.

REFERENCES

Apkarian, P. and Noll, D. (2006). Nonsmooth H∞ synthesis. *IEEE Transactions on Automatic Control*, 51(1), 71–86. doi:10.1109/TAC.2005.860290.

Barth, J.M.O., Condomines, J.P., Bronz, M., Hattenberger, G., Moschetta, J.M., Join, C., and Fliess, M. (2020). Towards a unified model-free control architecture for tailsitter micro air vehicles: Flight simulation analysis and experimental flights. In *AIAA Scitech 2020 Forum*. AIAA. doi:10.2514/6.2020-2075. URL `https://hal-enac.archives-ouvertes.fr/hal-02549682`.

Bronz, M., Tal, E., Favalli, F., and Karaman, S. (2020). Mission-Oriented Additive Manufacturing of Modular Mini-UAVs. In *AIAA Scitech 2020 Forum*, AIAA Scitech 2020 Forum. AIAA, Orlando, United States. doi:10.2514/6.2020-0064. URL `https://hal-enac.archives-ouvertes.fr/hal-02982370`.

Ducard, G.J.J. and Allenspach, M. (2021). Review of designs and flight control techniques of hybrid and convertible VTOL UAVs. *Aerospace Science and Technology*, 118, 107035. doi:10.1016/j.ast.2021.107035.

Huang, M. and Wang, Z.w. (2015). A Review of Wind Tunnel Based Virtual Flight Testing Techniques for Evaluation of Flight Control Systems. *International Journal of Aerospace Engineering*, 2015, e672423. doi:10.1155/2015/672423. Publisher: Hindawi.

LabJack (2001). T7. URL `https://labjack.com/products/t7`. Accessed: 2022-09-19.

Lustosa, L.R., Defaÿ, F., and Moschetta, J.M. (2019). Global Singularity-Free Aerodynamic Model for Algorithmic Flight Control of Tail Sitters. *Journal of Guidance, Control, and Dynamics*, 42(2), 303–316. doi:10.2514/1.G003374.

Olszanecki Barth, J.M., Condomines, J.P., Bronz, M., Moschetta, J.M., Join, C., and Fliess, M. (2020). Model-free control algorithms for micro air vehicles with transitioning flight capabilities. *International Journal of Micro Air Vehicles*, 12, 1–22. doi:10.1177/1756829320914264.

Saeed, A.S., Younes, A.B., Cai, C., and Cai, G. (2018). A survey of hybrid Unmanned Aerial Vehicles. *Progress in Aerospace Sciences*, 98, 91–105. doi:10.1016/j.paerosci.2018.03.007.

Sansou, F. (2022). Commande hybride d'un drone convertible pour des déplacements sous optimaux. doi:10.48550/ARXIV.2203.15387. URL `https://arxiv.org/abs/2203.15387`.

Sansou, F. and Zaccarian, L. (2022). On local-global hysteresis-based hovering stabilization of the DarkO convertible UAV. In *2022 European Control Conference (ECC)*, 40–45. doi:10.23919/ECC55457.2022.9838387.

Silva, N., Fontes, J., Inoue, R., and Branco, K. (2018). Dynamic inversion and gain-scheduling control for an autonomous aerial vehicle with multiple flight stages. *Journal of Control, Automation and Electrical Systems*, 29(3), 328–339.

Smeur, E.J.J., Bronz, M., and de Croon, G.C.H.E. (2019). Incremental control and guidance of hybrid aircraft applied to the Cyclone tailsitter UAV. *Journal of Guidance, Control, and Dynamics*. doi:10.2514/1.G004520.

Tal, E. and Karaman, S. (2022). Global incremental flight control for agile maneuvering of a tailsitter flying wing. *arXiv preprint arXiv:2207.13218*.